Driver Circuit Design for a New Eddy Current Sensor in Displacement Measurement of Active Magnetic Bearing Systems

Cao, Zhi; Huang, Yunkai; Peng, Fei; Dong, Jianning

DOI
10.1109/JSEN.2022.3194567

Publication date
2022

Document Version
Final published version

Published in
IEEE Sensors Journal

Driver Circuit Design for a New Eddy Current Sensor in Displacement Measurement of Active Magnetic Bearing Systems

Zhi Cao, Yunkai Huang, Fei Peng, and Jianning Dong, *Senior Member, IEEE*

***Abstract*—Position sensing is one of the crucial parts of the active magnetic bearing (AMB) system. The printed circuit board (PCB) eddy current position sensor is a new type of position sensor for the AMB system, which makes a compact structure, high sensing quality, and is low cost. In this article, an improved driver circuit is proposed for this new sensor. The driver circuit includes an excitation circuit and signal conditioning circuits. A crystal oscillator circuit with a power stage is used to provide the excitation coil with a stable excitation source of high stability and good precision of frequency. The analog demodulation circuit is designed for signal conditioning circuits to extract the rotor displacement information from the sensing coil outputs. Compared with the state-of-art driver schemes, the proposed method reduces the circuit complexity and cost. Accordingly, the experimental results show that the designed sensor has good linearity and sensitivity, and it can ensure AMB stable operation at the rated speed.**

***Index Terms*—Active magnetic bearing (AMB), driver circuit, eddy current sensor, position measurement.**

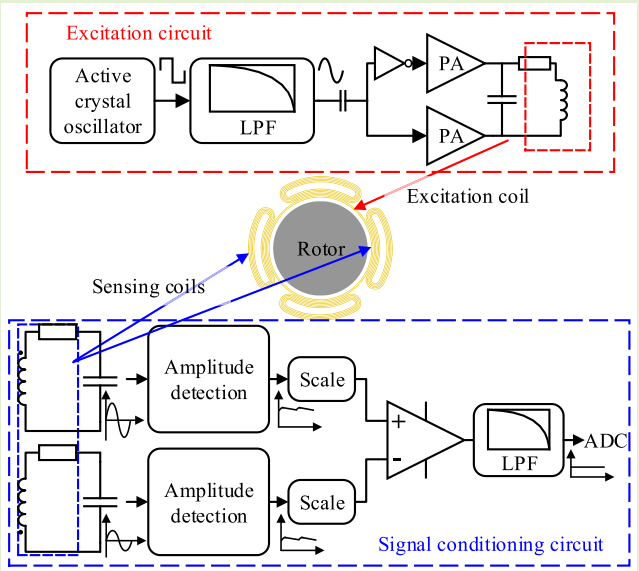

I. Introduction

THE active magnetic bearing (AMB) has attractive features such as no contact between rotor and stator, no lubrication needed, no mechanical wear, extended lifespan, and the ability to actively control rotor dynamics [1]. Therefore, it is favorable and promising in many critical high-speed industrial applications, where conventional mechanical bearings have a limited life span.

Rotor position measurement is a key part in the AMB system, and two prominent techniques of obtaining the rotor position are self-sensing and dedicated noncontact sensors [2]. The self-sensing approach abandons the integration of physical position sensors and extracts the position information from the electromagnetic signals in the bearing actuators [3]–[5]. However, it is most often at the expense of a loss of system robustness and increased controller complexity [2], [6]. Most dedicated state-of-the-art AMBs still use dedicated position sensors, usually including inductive and eddy current sensors. These position sensors could provide the rotor displacement information accurately and quickly. A 5-DOF AMB system, as shown in Fig. 1, needs multiple sensors (at least five; even ten for the differential measurement) to obtain the rotor displacement in each direction [7], [8], which is high cost and space-consuming.

Bühler proposed a printed circuit board (PCB) sensor for the rotor radial displacement based on the eddy current effect [9]. The coils are etched on the PCB, replacing the sensor probe of the conventional sensor. Such a design allows a compact design of the AMB system, guarantees sensor uniformity, reduces the cost, and avoids the synchronization problem of multiple sensor probes [17]. This sensor is also called a transverse flux sensor (TFS) in [10] since it uses the transversal

Manuscript received 30 March 2022; revised 28 June 2022 and 22 July 2022; accepted 25 July 2022. Date of publication 3 August 2022; date of current version 1 September 2022. This work was supported in part by the National Natural Science Foundation of China under Grant 51777034 and Grant 52037002. The associate editor coordinating the review of this article and approving it for publication was Dr. Ferran Reverter. *(Corresponding author: Yunkai Huang.)*

Zhi Cao, Yunkai Huang, and Fei Peng are with the School of Electrical Engineering, Southeast University, Nanjing 210096, China (e-mail: caozhi@seu.edu.cn; huangyk@seu.edu.cn; pengfei@seu.edu.cn).

Jianning Dong is with the Department of Electrical Sustainable Energy, Delft University of Technology, 2628 Delft, The Netherlands (e-mail: j.dong-4@tudelft.nl).

Digital Object Identifier 10.1109/JSEN.2022.3194567

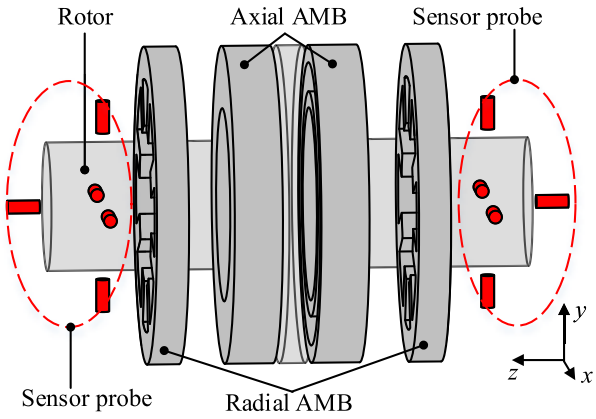

Fig. 1. 5-DOF AMB system.

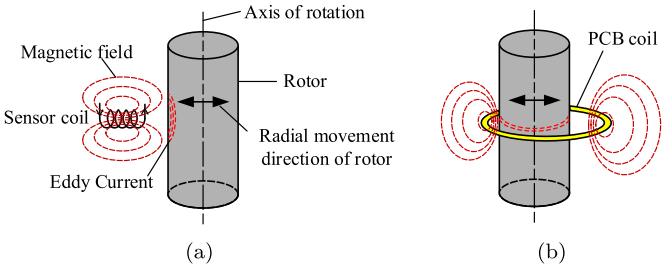

Fig. 2. Layout of eddy current sensors. (a) Conventional configuration. (b) TFS.

field variation to detect the rotor movement. In contrast, the traditional eddy current sensor uses the vertical field variation. The layout comparison between the conventional eddy current sensor and the TFS is shown in Fig. 2. The TFS is further developed for high-temperature AMBs using the thick-film manufacturing techniques in [11]. Furthermore, the sensor is modeled by different methods including the 2-D finite element model (FEM) [12], [13], 3-D FEM [14], and partial element equivalent circuit (PEEC) method [15], and optimal design laws for the TFS are summarized by comprehensively analyzing various parameters regarding the sensor performance.

Niemann develops a high-precision driver for the TFS in [16]. The sensor driver mainly includes a sensor excitation circuit, a signal conditioning circuit, and the subsequent digital processing circuit. A direct digital synthesis (DDS) chip could perform a wide range of simple and complex modulation schemes and is chosen to generate the excitation signal in [16]. However, it increases the cost and circuit complexity. The signal conditioning circuit in [10] applies direct digital demodulation and filtering scheme. This scheme requires extremely high-speed analog-to-digital converters (ADCs) and a very high-throughput rate, resulting in a heavy burden on digital processing. In addition, this scheme needs to detect both the amplitude and phase of the output signal.

This article focuses on a simpler and more convenient configuration for the TFS driver to improve production efficiency. To simplify the sensor circuit and reduce the difficulty of configuration, this article proposes a totally analog design of the sensor driver based on the fixed frequency oscillator and analog demodulation.

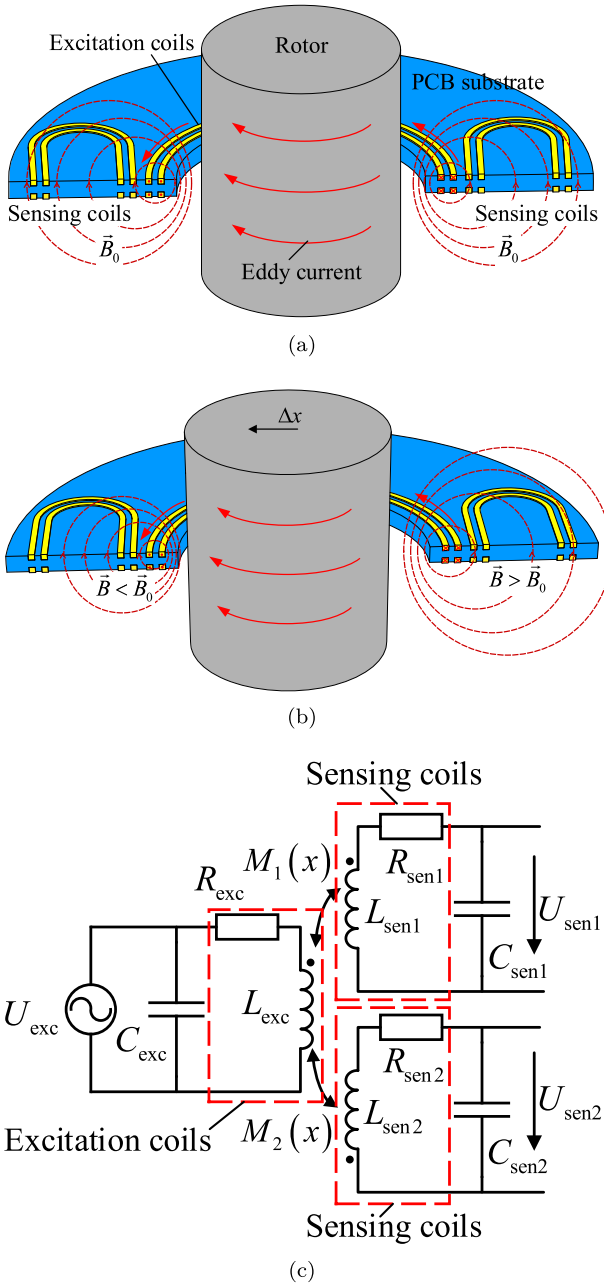

Fig. 3. Principle of TFS for position detection with (a) centered rotor and (b) eccentric rotor. (c) Equivalent circuit of the TFS.

The article is organized as follows. The principle of TFS detecting the rotor position is first introduced in Section II. In Section III, the design of the improved driver circuit is depicted in detail. The results from the experimental setup are described in Section IV. Finally, Section V concludes this article.

II. Sensor Theory

The principle of the transverse flux displacement sensor is shown in Fig. 3. The TFS consists of a PCB and a central rotor target, and there is an excitation coil wound around the rotor on the PCB and four sensing coils surrounding the excitation coil. Driven by a high-frequency voltage or current, the excitation coil generates a concentric magnetic field and

induces voltages in the four sensing coils. The rotor is electrically conductive and weakens the excitation magnetic field by an eddy current around its axis. The induced voltages in the opposing sensing coils are equal when the rotor is centered as shown in Fig. 3(a) due to the symmetry of the structure. When the rotor is displaced laterally from the center position as shown in Fig. 3(b), the magnetic field distribution in the opposing sensing coils becomes asymmetric since the field generated by the rotor eddy current becomes asymmetric and superposed with the excitation field. Therefore, the induced voltage difference between two opposing sensing coils could indicate the rotor displacement.

The TFS can be modeled by an equivalent transformer circuit as depicted in Fig. 3(c). L_{exc}, L_{sen1}, and L_{sen2} are the inductance of the excitation coil and two opposing sensing coils, respectively; R_{exc}, R_{sen1}, and R_{sen2} are the resistance of the excitation coil and two opposing sensing coils, respectively; $M_1(x)$ and $M_2(x)$ are the mutual inductance between the excitation coil and two opposing sensing coils, respectively. The capacitors C_{exc}, C_{sen1}, and C_{sen2} are added to form the resonant circuits and provide extra gain for the sensor. The output voltage difference U_{diff} of two opposing sensing coils is given by [15]

$$U_{\text{diff}} = U_{\text{sen1}} - U_{\text{sen2}} = \frac{j\omega M_{\text{diff}} I_{\text{exc}}}{j\omega R_{\text{sen}} C_{\text{sen}} - \omega^2 L_{\text{sen}} C_{\text{sen}} + 1} \tag{1}$$

where $M_{\text{diff}} = M_1 - M_2$; $R_{\text{sen}} = R_{\text{sen1}} = R_{\text{sen2}}$, $L_{\text{sen}} = L_{\text{sen1}} = L_{\text{sen2}}$, and $C_{\text{sen}} = C_{\text{sen1}} = C_{\text{sen2}}$ due to the symmetry of the opposing coils; and I_{exc} is given as

$$I_{\text{exc}} = \frac{U_{\text{exc}}}{j\omega L_{\text{exc}}} \tag{2}$$

when an ac voltage source is applied to the excitation coil, which could increase the sensor sensitivity [17].

The resonant frequency in (1) can be calculated as

$$f_{\text{res}} = \frac{1}{2\pi\sqrt{L_{\text{sen}} C_{\text{sen}}}}. \tag{3}$$

When the sensor works at the resonant frequency, the sensitivity can be expressed as

$$S = \frac{\mathrm{d}U_{\text{diff}}}{\mathrm{d}x} = \omega_{\text{exc}} U_{\text{exc}} \frac{L_{\text{sen}}}{L_{\text{exc}} R_{\text{sen}}} \frac{\mathrm{d}M_{\text{diff}}}{\mathrm{d}x}. \tag{4}$$

The TFS model of (1)–(4) has been developed and investigated in [15] by the PEEC method. A further and thorough analysis of the various influence factors on the sensitivity is conducted in [13] and [14] using the 2-D and 3-D FEM, respectively. The used TFS design in this article is proposed according to the analysis in [14], and it is specified in Table I.

TABLE I
PARAMETERS OF THE USED TFS

Parameter	Value
Rotor material	Aluminum alloy
Rotor diameter	28.4mm
PCB center hole diameter	31.4mm
Tack width	0.127mm(5mil)
Track clearance	0.127mm(5mil)
Track copper thickness	0.089mm(1oz)
PCB substrate thickness	12mm
Excitation frequency	6MHz
Excitation coil inductance L_{exc}	3.085μH
Excitation coil resistance R_{exc}	4.5Ω
Excitation coil quality factor Q_{exc}	25.884
Sensing coil inductance L_{sen}	3.86μH
Sensing coil resistance R_{sen}	4.6Ω
Sensing coil quality factor Q_{sen}	31.666
Excitation voltage amplitude U_{exc}	24V
$\mathrm{d}M_{\text{diff}}/\mathrm{d}x$	0.0416μH/μm

III. Driver Circuit Design

The designed sensor driver is illustrated in Fig. 4, and it consists of a sensor excitation circuit, a PCB sensor, a signal conditioning circuit, and the subsequent sampling and processing circuit. This article focuses on the analog design of the sensor driver.

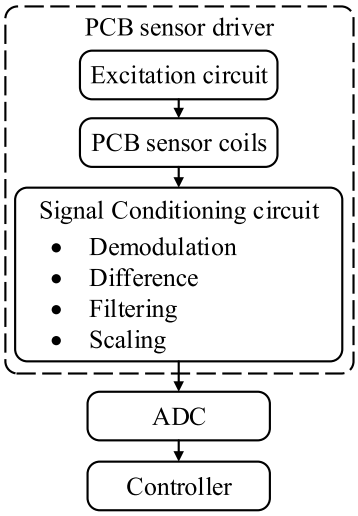

Fig. 4. Overall diagram of the designed sensor driver.

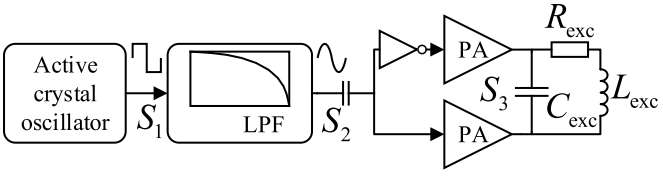

Fig. 5. Excitation circuit.

A. Excitation Circuit

The designed excitation circuit is shown in Fig. 5. It works as an ac constant voltage source to provide a voltage input with the resonant frequency to the excitation coil. The excitation source needs to be accurate and stable. Any variation in the excitation signal will result in a variation in the sensor output signal, causing erroneous position readings and faulty control of the AMB. The traditional oscillation circuit for eddy current sensors such as the Colpitts oscillator is sensitive to the circuit parameters [18]. Considering the frequency stability and easy realization of the circuit, an active crystal oscillator is used to generate the excitation signal due to its high quality

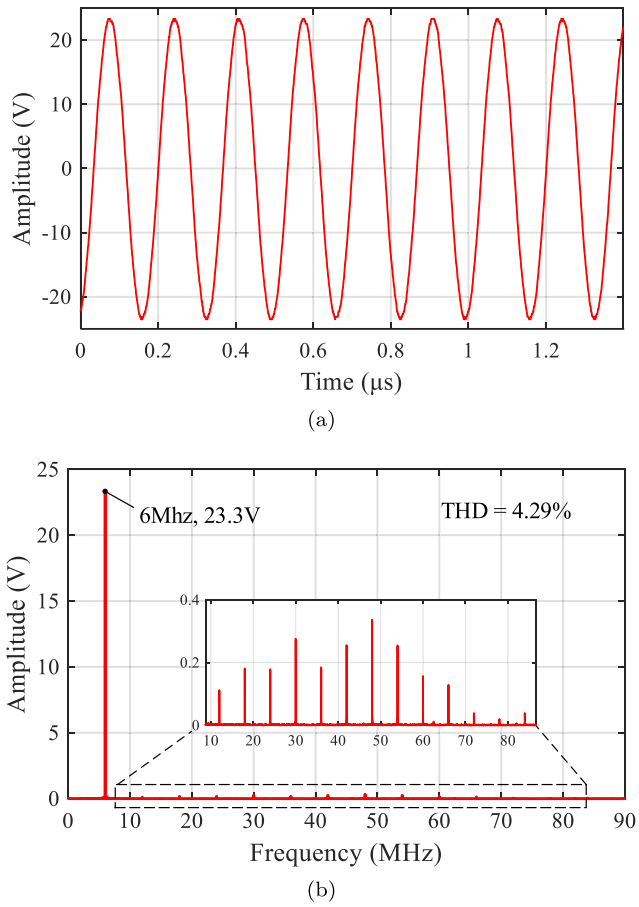

Fig. 6. Measured signal S_3. (a) Waveform. (b) Frequency spectrum.

factor. The square wave signal (S_1) generated by the active crystal oscillator is first passed through a second-order active low-pass filter to generate a sinusoidal signal (S_2); then the sinusoidal signal (S_2) is converted into a pair of differential signals fed to the power amplifiers (PAs), and the excitation signal has enough energy to generate eddy current in the rotor. Such a differential drive circuit doubles the swing range of the excitation voltage and therefore increases the sensor sensitivity. The capacitor C_{exc} is in parallel with the excitation coil to alleviate the output current of the PAs. Fig. 6(a) shows the waveform of the signal S_3 applied to the excitation coil, and Fig. 6(b) presents its frequency spectrum. The signal S_3 is measured at varying rotor positions and is found to be constant throughout. The amplitude stability of the excitation circuit is thus guaranteed.

B. Signal Conditioning Circuit

The induced voltage signals from the sensing coils are fed to the signal conditioning circuit as shown in Fig. 7. These sensing signals are demodulated, filtered, differentially operated, and scaled to the proper range for the ADCs. The resonant circuit formed by the sensing capacitor C_{sen} and the sensing coil could significantly increase the sensing signal amplitude and suppress the nonexcitation frequency signal components. However, the sensing capacitor in this article is selected such that the sensor operates slightly off the

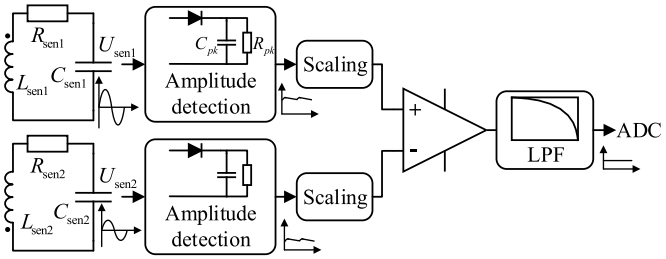

Fig. 7. Signal conditioning circuit.

resonant frequency to reduce the sensitivity of the output to the component parameter variation and to keep the sensing signal relatively stable. Meanwhile, it would cause some signal amplitude loss.

It can be seen from (1) that the amplitude variation in the sensing voltage reflects the rotor position variation. Therefore, amplitude demodulation is necessary. A simple amplitude detection circuit shown in Fig. 7 is constructed using a diode, a resistor, and a capacitor to convert the sinusoidal sensing signal into a dc value. According to [19], the amplitude detection capacitor C_{pk} and resistor R_{pk} are selected to satisfy for

$$\frac{\Delta u}{\omega_c} \le R_{\text{pk}} C_{\text{pk}} \le \frac{\sqrt{1-m^2}}{\omega_m m} \tag{5}$$

where ω_c is the carrier frequency, i.e., the excitation frequency in this article; ω_m is the modulation frequency; Δu is the required normalized output ripple in %; and m is the modulation index.

The sensing voltage amplitude in our design exceeds the input range of the ADCs, so a resistor divider network is used here to scale down the amplitude demodulation circuit output. Next, the amplitude difference between two opposing sensing coils is obtained by the subtractor, and it is then passed through an anti-alias filter and ready for sampling by ADCs.

The dynamic property of the sensor is determined by the dynamics of the amplitude detector and the anti-alias filter before ADC [20], and it is given by

$$H_s(j\omega) = H_{\text{pk}}(j\omega) H_{\text{lp}}(j\omega) = \frac{1 - \frac{1}{2 f_c R_{\text{pk}} C_{\text{pk}}}}{1 + \frac{j\omega}{2 f_c}} H_{\text{lp}}(j\omega) \tag{6}$$

where $H_{\text{pk}}(j\omega)$ and $H_{\text{lp}}(j\omega)$ are the transfer functions of the amplitude detector and anti-alias filter, respectively.

IV. Experiments

Several tests are conducted to evaluate the performance of the designed TFS in this section. A static calibration platform as shown in Fig. 8(a) is built for the sensor's static characteristics test and calibration. The 2-D translation calibration platform can move the measured rotor with a step of 0.01 mm. The oscilloscope is used to measure the sensor output signal. Afterward, TFS is integrated into an AMB system, as shown in Fig. 8(b), for the static suspension and rotation experiments.

The component parameters of the designed sensor driver are shown in Table II.

The anti-alias filter in this article is a second-order low-pass Butterworth filter, and its −3-dB cut-off frequency is designed

TABLE II
PARAMETERS OF THE DESIGNED SENSOR

Parameter	Value
Excitation capacitor C_{exc}	240 pF
Sensing capacitor C_{sen}	160 pF
Amplitude detector capacitor C_{pk}	10 pF
Amplitude detector resistor R_{pk}	1.0523 MΩ
Amplitude detector diode	1N4148W T4

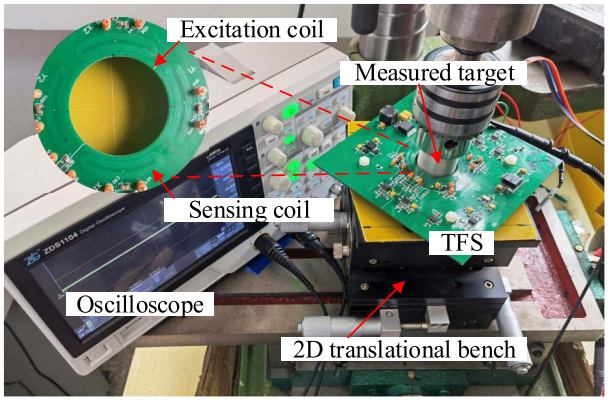

(a)

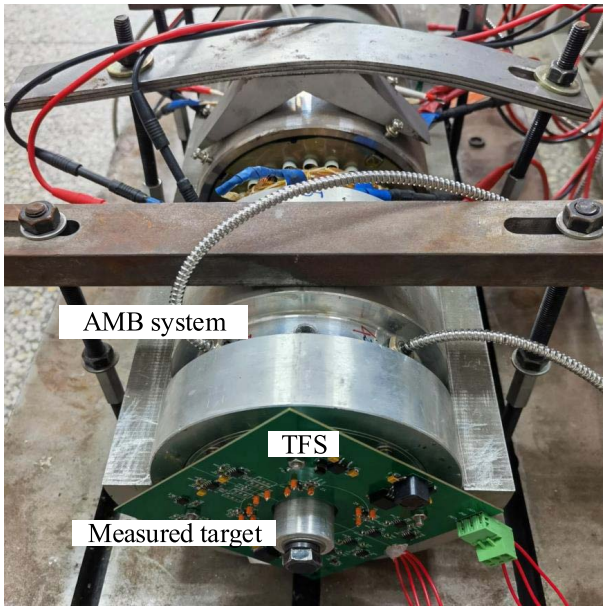

(b)

Fig. 8. Experimental setup. (a) Static calibration platform. (b) AMB system with TFS.

at 10 kHz. According to (6) and the parameters in Table II, the magnitude and phase frequency response of the designed sensor are presented in Fig. 9.

A. Static Characteristics Test

The TFS can measure two radial displacements simultaneously. The measuring range of the designed sensor is ±1.4 mm. The rotor is centered in one direction and moved in the orthogonal direction. The designed sensor is measured four times in two opposite stepping directions (i.e., from

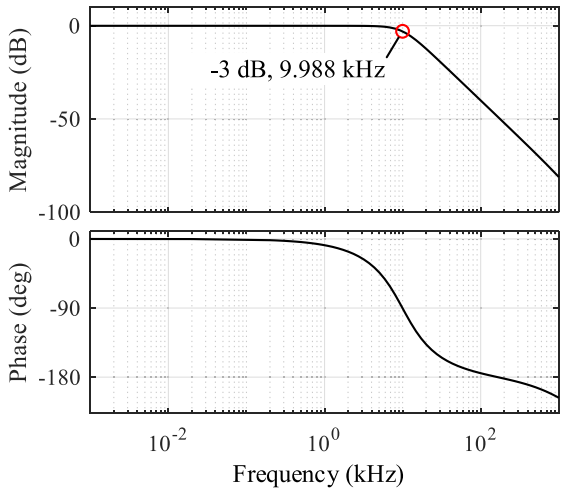

Fig. 9. Magnitude and phase frequency response of the designed sensor.

TABLE III
PERFORMANCE SPECIFICATION

Specification	X direction	Y direction
Sensitivity	1.143 V/mm	1.201V/mm
Linearity	5.08%	5.21%
Repeatability	0.32%	0.64%

−1.4 mm to +1.4 mm and from +1.4 mm to −1.4 mm), respectively. Fig. 10 shows the output characteristics $U_x(x)$ and $U_y(y)$ of the designed sensor in two orthogonal directions, respectively. The corresponding performance specification is listed in Table III.

As the rotor displaces in one direction, the output voltage of the other direction remains almost constant, and the slight variation is introduced by mechanical assembly error and some little differences in circuit parameters between the two sensing coils. Therefore, the outputs of the X and Y directions are decoupled.

The scaling factor of the conditioning circuit is 0.211 in this design, and the theoretical sensitivity calculated by (4) after scaling should be 1.467 V/mm. It can be seen from the test results that the sensor actually has a sensitivity of 1.143 and 1.201 V/mm in the X and Y directions, which are lower than the theoretical value. This is because we choose the sensing capacitors that make the sensor work beside the resonant frequency to keep the sensing signal stable. Thus, the actual output sensitivity is decreased compared with the theoretical value. Also, this might be attributed to factors such as PCB manufacturing imperfection and distribution parameters of wiring.

Besides, the above non-ideal factors cause differences in the performance of the two directions.

B. Work Test

The sensor is further mounted on an AMB system to prove that the designed sensor could ensure the normal operation of the AMB system. The output signals of the designed sensor

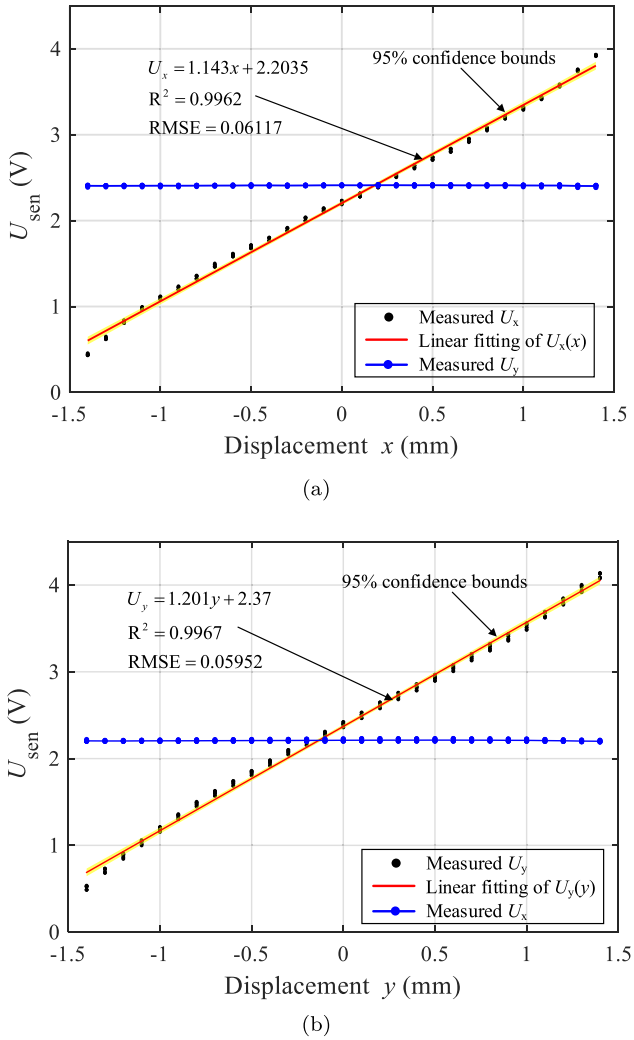

Fig. 10. Static output characteristics of TFS in (a) *X*-direction and (b) *Y*-direction.

are fed into the controller, and a static suspension experiment and rotational suspension experiments are carried out.

With the designed sensor incorporated into the control system, the rotor can be stably suspended near the center position. Fig. 11 shows the output signals of the designed sensor under the rotor stationary suspension. According to the static input–output characteristic equations in Fig. 10, the unit of the sensor output is converter to mm here. The peak-to-peak values of the sensor signal in the X and Y directions are 32 and 27 μm (8% and 6.75% of the maximum range), respectively.

Further rotational experiments proceed with the designed sensor, and the stable rotor suspension up to 6000 r/min is achieved. Fig. 12 shows the rotor orbits from the sensor output signals. The rotor displacement range is within ± 250 μm. It should be noted that the rotor lateral displacement is closely related to control algorithms and the sensor performance. Since the sensor is mounted at the end of the shaft, the measured surface has obvious run-out, which can be observed from the rotor orbits in Fig. 12. , From the test data above, it can be concluded that the designed sensor can ensure reliable operation of the AMB system.

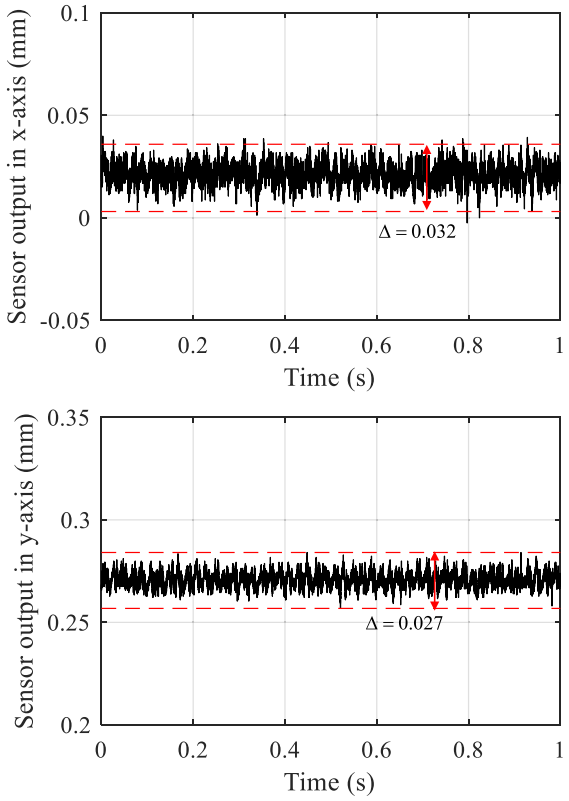

Fig. 11. Sensor outputs under rotor static suspension experiment.

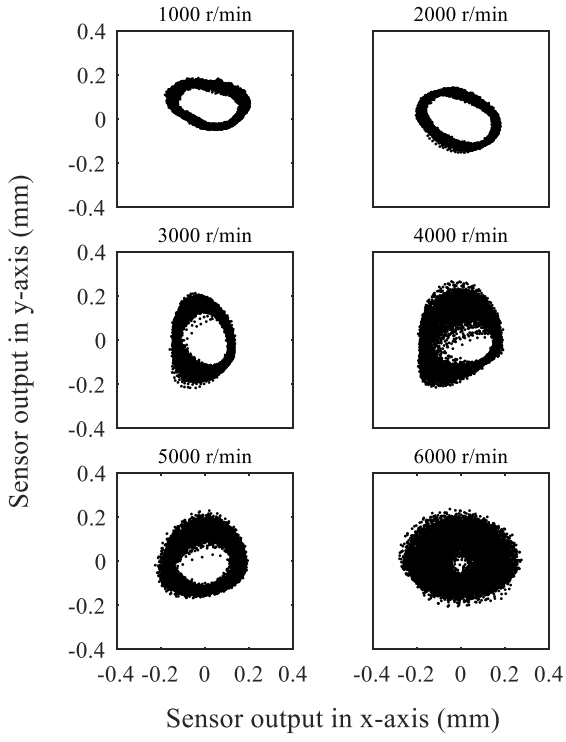

Fig. 12. Rotor orbits plotted from sensor output signals with different rotation speeds.

V. Conclusion

This article presented an improved drive circuit for the PCB eddy current position sensor. A crystal oscillator circuit with a power stage is designed as the excitation circuit to improve

the stability and consistency of the excitation signal. A simple analog demodulation circuit is applied to extract the rotor displacement signals. The demodulation circuit can output a dc voltage signal, which is proportional to the displacement. By static characteristic tests, the proposed sensor design shows good linearity and sensitivity. The dynamic work test results show that the magnetic bearing rotor can be stably operated up to 6000 r/min. The driver circuit is simple, low-cost, and reliable.

REFERENCES

[1] G. Schweitzer and E. H. Maslen, *Magnetic Bearings: Theory, Design, and Application to Rotating Machinery*. Berlin, Germany: Springer, Jun. 2009.

[2] R. Larsonneur and P. Bühler, "New radial sensor for active magnetic bearings," in *Proc. 9th Int. Symp. Magn. Bearings*, Lexington, KY, USA, 2004, pp. 495–499.

[3] D. Vischer and H. Bleuler, "Self-sensing active magnetic levitation," *IEEE Trans. Magn.*, vol. 29, no. 2, pp. 1276–1281, Mar. 1993.

[4] Y. Jiang, K. Wang, M. Sun, and J. Xie, "Displacement self-sensing method for AMB-rotor systems using current ripple demodulations combined with PWM command signals," *IEEE Sensors J.*, vol. 19, no. 14, pp. 5460–5469, Jul. 2019.

[5] Z. Ren, H. Li, X. Chen, W. Yu, and R. Chen, "Impedance modeling of self-inductive displacement sensor considering iron core reluctance and flux leakage," *IEEE Sensors J.*, vol. 22, no. 9, pp. 8583–8595, May 2022.

[6] J. Sun and H. Zhu, "Self-sensing technology of rotor displacement for six-pole radial active magnetic bearing using improved quantum particle swarm optimized cubature Kalman filter," *IEEE J. Emerg. Sel. Topics Power Electron.*, vol. 10, no. 3, pp. 2881–2889, Jun. 2022.

[7] S. E. Mushi, Z. Lin, and P. E. Allaire, "Design, construction, and modeling of a flexible rotor active magnetic bearing test rig," *IEEE/ASME Trans. Mechatronics*, vol. 17, no. 6, pp. 1170–1182, Dec. 2012.

[8] P. Peralta, S. Thomas, and Y. Perriard, "Characterization and verification of eddy-current position sensing for magnetic levitation," *IEEE Trans. Ind. Appl.*, vol. 57, no. 6, pp. 5796–5805, Nov. 2021.

[9] P. Bühler, "Device for contact-less measurement of distances in multiple directions," E.P. Patent EP1 422 492A1, May 2004.

[10] C. M. Zingerli, P. Imoberdorf, J. W. Kolar, and T. Nussbaumer, "Rotor position measurement for a magnetically levitated 500'000 RPM permanent magnet machine," in *Proc. IEEE Energy Convers. Congr. Exp.*, Sep. 2011, pp. 1778–1784.

[11] L. Burdet, T. Maeder, R. Siegwart, P. Bühler, and B. Aeschlimann, "Thick-film radial position sensor for high temperature active magnetic bearings," in *Proc. 10th Int. Symp. Magn. Bearings*, Jan. 2006, pp. 1–5.

[12] A. J. Grobler, "A low cost eddy current displacement sensor for active magnetic bearings," M.S. thesis, School Elect., Electron. Comput. Eng., North-West Univ., Potchefstroom, South Africa, 2008.

[13] A. Grobler, G. Van Schoor, and E. Ranft, "Design and optimization of a PCB eddy current displacement sensor," *SAIEE Afr. Res. J.*, vol. 108, no. 1, pp. 4–11, 2017.

[14] L. Xue, K. Zhang, and Y. Xu, "Research on new displacement sensor used in active magnetic bearing systems," in *Proc. Int. Symp. Softw. Rel., Ind. Saf., Cyber Secur. Phys. Protection Nucl. Power Plant*. Singapore: Springer, 2017, pp. 174–187.

[15] A. Müesing, C. Zingerli, P. Imoberdorf, and J. W. Kolar, "PEEC-based numerical optimization of compact radial position sensors for active magnetic bearings," in *Proc. 5th Int. Conf. Integr. Power Electron. Syst.*, 2008, pp. 1–5.

[16] H. E. Niemann, "A high precision driver for an eddy current displacement sensor," M.S. thesis, School Elect., Electron. Comput. Eng., North-West Univ., Potchefstroom, South Africa, 2009.

[17] L. Xue, "Research on measurement and control system of active magnetic bearings," M.S. thesis, Dept. Eng. Phys., Tsinghua Univ., Beijing, China, 2018.

[18] M. Sun, J. Zhou, B. Dong, and S. Zheng, "Driver circuit improvement of eddy current sensor in displacement measurement of high-speed rotor," *IEEE Sensors J.*, vol. 21, no. 6, pp. 7776–7783, Mar. 2021.

[19] P. Pejović. *Peak Detector and/or Envelope Detector—A Detailed Analysis*. Accessed: Aug. 5, 2022. [Online]. Available: https://zenodo.org/record/1310694

[20] T. Sillanpää *et al.*, "Three-axis inductive displacement sensor using phase-sensitive digital signal processing for industrial magnetic bearing applications," *Actuators*, vol. 10, no. 6, p. 115, May 2021.

Zhi Cao received the B.E. degree in electrical engineering from Southeast University, Nanjing, China, in 2016, where he is currently pursuing the D.Eng. degree in electric machines and control with the School of Electrical Engineering.

His main research interests include design, analysis, and control of active magnetic bearing systems.

Yunkai Huang received the M.Sc. and Ph.D. degrees in electrical engineering from Southeast University, Nanjing, China, in 2001 and 2007, respectively.

He is currently a Professor with the School of Electrical Engineering, Southeast University, where he is teaching Electrical Machinery and Digital Signal Processing. His research interests include design and control of PM machine and high-speed machine, applications in domestic appliances, electric vehicles, railway traction, all-electric ships, and wind power generation systems.

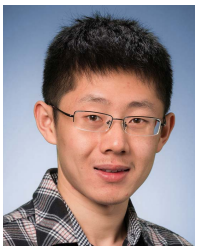

Fei Peng received the B.S. and M.S. degrees in electrical engineering from Southeast University, Nanjing, China, in 2010 and 2012, respectively, and the Ph.D. degree in electrical and computer engineering from McMaster University, Hamilton, ON, Canada, in 2016.

After that, he was a Postdoctoral Fellow with the McMaster Institute for Automotive Research and Technology, McMaster University. In December 2016, he joined the School of Electrical Engineering, Southeast University, as an Assistant Professor. His research interests include optimal design and control of power converters, modeling, and digital control of motor drives.

Jianning Dong (Senior Member, IEEE) received the B.S. and Ph.D. degrees in electrical engineering from Southeast University, Nanjing, China, in 2010 and 2015, respectively.

Since 2016, he has been an Assistant Professor with the Delft University of Technology (TU Delft), Delft, The Netherlands, where he is teaching Electromechanics. Before joining TU Delft, he was a Postdoctoral Researcher with the McMaster Automotive Resource Centre, McMaster University, Hamilton, ON, Canada. His main research interests include design, modeling, and control of electromechanical systems.